Pergamon

0038-1101(95)00162-X

Solid-State Electronics Vol. 39, No. 4, pp. 583–592, 1996

0038-1101/96 $15.00 + 0.00

BARRIER CHARACTERISTICS OF PtSi/*p*-Si SCHOTTKY DIODES AS DETERMINED FROM *I–V–T* MEASUREMENTS

P. G. McCAFFERTY[1], A. SELLAI[1]†, P. DAWSON[1] and H. ELABD[2]

[1]Department of Pure and Applied Physics, Queen's University of Belfast, Belfast BT7 1NN, U.K.
[2]Loral Fairchild Imaging Systems, 1801 McCarthy Boulevard, Milpitas, CA 95035, U.S.A.

(Received 23 December 1994; in revised form 14 July 1995)

Abstract—The current–voltage–temperature characteristics of PtSi/*p*-Si Schottky barrier diodes were measured in the temperature range 60–115 K. Deviation of the ideality factor from unity below 80 K may be modelled using the so-called T_0 parameter with $T_0 = 18$ K. It is also shown that the curvature in the Richardson plots may be remedied by using the *flatband* rather than the *zero-bias* saturation current density. Physically, the departure from ideality is interpreted in terms of an inhomogeneous Schottky contact. Here we determine a mean barrier height at $T = 0$ K, $\bar{\phi}_b^0 = 223$ mV, with an (assumed) Gaussian distribution of standard deviation $\sigma_\phi = 12.5$ mV. These data are correlated with the zero-bias barrier height, $\phi_j^0 = 192$ mV (at $T = 90$ K), the photoresponse barrier height, $\phi_{ph} = 205$ mV, and the flatband barrier height, $\phi_{fb} = 214$ mV. Finally, the temperature coefficient of the flatband barrier was found to be -0.121 mV K^{-1}, which is approximately equal to $1/2(dE_g^i/dT)$, thus suggesting that the Fermi level at the interface is pinned to the middle of the band gap.

INTRODUCTION

There is currently a vast number of reports of experimental studies of barrier heights in a great variety of metal/semiconductor systems. The popularity of such studies, rooted in their importance to the semiconductor industry, does not, however, assure uniformity of results or of interpretation. For example, disagreements between the barrier heights from *C–V* measurements and those determined from *I–V* data are rarely reconciled; different groups, working with apparently similar samples under the same experimental conditions, obtain conflicting results. These comments are certainly true of the low-height Schottky barrier which is obtained at the PtSi/*p*-Si interface and is of considerable importance in photoemissive i.r. detector technology. Since these low barrier height devices must be operated at low temperatures to suppress the thermal dark current, one might anticipate that there would be a wealth of data on *I–V* characteristics as a function of temperature. Surprisingly this is not the case. Furthermore, from those reports that do address this matter, it is clear that there is no consensus of opinion with regard to the detailed description of the barrier or to the mechanism of carrier transport across the barrier. By way of introduction we give a brief survey of silicide/Si Schottky barriers and detail some of the points of differing interpretation below.

While the conduction processes in a silicide–semiconductor system are essentially the same as in a simple metal–semiconductor contact, differences are expected to occur which reflect the different interfacial properties. Some such differences have their origin with the crystallographic orientation of the substrate wafer. Using both electrical (current–voltage) and optical (internal photoemission) characterisation techniques, Pelligrini *et al.*[1] have demonstrated a difference in barrier height for PtSi/*p*-Si diodes grown on (111) and (100) substrates—diodes grown on (111) Si yield barrier heights up to 0.1 V higher than those grown on (100) substrates. Similar investigations on IrSi and $NiSi_2$ formed on *n*-type Si have revealed a barrier height dependence (of up to 0.13 V) on substrate crystallographic orientation[2,3]. Tanabe *et al.*[4] studied the influence of Fermi-level pinning on barrier inhomogeneity in PtSi/*p*-Si Schottky contacts. Using a modified Fowler analysis to explain their experimental photoemission data they argued for the co-existence of two regions with discretely different barrier heights. Guttler and Werner[5] have explained the origin of noise in silicide/Si Schottky detectors in terms of barrier height inhomogeneity due to spatial fluctuations in the density of interface states. Central to this interpretation was the experimentally observed increase in barrier height with increasing temperature. Those authors subsequently carried out a more rigorous development of their ideas on barrier height inhomogeneities with reference to a broad range of diode types[6] and showed that the curvature of the

†Present address: Universite Ferhat Abbas, Institut de Physique, 19000 Setif, Algeria.

Richardson plots and temperature dependent ideality factor n obtained from I–V–T measurements allows for a quantitative characterisation of spatial inhomogeneities at Schottky contacts[6,7]. By contrast, Aboelfotoh[8], who studied several different types of silicide/Si Schottky diodes using both I–V–T ($77\,\mathrm{K} < T < 295\,\mathrm{K}$) and C–V measurements, obtained results which deviated significantly from those of Guttler and Werner[5–7]. The variation of Schottky barrier height with temperature was explained in terms of Fermi level pinning relative to the Si valence band edge.

The work most closely related to the present study is that of Chin *et al.*[9,10]. In their earlier work[9] these authors reported I–V–T results in the temperature range 80–120 K which they interpreted in terms of a Gaussian potential distribution for the Schottky barrier—they reported a mean barrier height of 242 mV of standard deviation 11 mV. More recently the same authors[10] reported a similar study, again on PtSi/p-Si devices, over a broader temperature range of 80–160 K. In the temperature region 80–110 K the current contribution from the barrier distribution was considered to be negligible and the results were explained using pure thermionic emission theory. Above 110 K there was a sudden drop in the barrier height and from 110–150 K, current flow was modelled using thermionic emission diffusion theory. Beyond 150 K, diffusion current was considered to be the dominant current mechanism in these PtSi/p-Si diodes.

In this report we present I–V–T measurements in the temperature range 60–115 K on PtSi/p-Si diodes. The extension of the lower limit of the temperature range to 60 K, 20 K lower than that used by Chin *et al.*[9,10], means that our results usefully complement those of Chin *et al.* For example, it is only for $T < 80\,\mathrm{K}$ that the ideality factor shows a strong variation with temperature. In considering our results we start from the basis of simple thermionic emission theory. The problems arising in this approach are then addressed in an essentially empirical manner in the context of modified thermionic models. First, we present an analysis in terms of the so-called T_0-parameter; next, we apply to our results a model which uses the flatband rather than the zero-bias current density. In developing a more physically-based interpretation of the departure from ideal behaviour we find that the salient features of the experimental I–V–T data can be explained in terms of a distribution in the Schottky barrier height.

DIODE FABRICATION AND EXPERIMENT

The PtSi/p-Si Schottky diodes used in this study were 0.64 mm^2 test diodes fabricated around the edge of large area diodes which were prepared by Loral Fairchild Imaging Systems (Milpitas) for optical analysis using a prism coupling technique[11,12]. The substrate is p-type Si of ⟨100⟩ orientation, with doping concentration of 10^{14}–$10^{15}\,\mathrm{cm}^{-3}$. Guard rings were used around the periphery of the diodes to prevent edge leakage. Cleaning of the wafers, platinum evaporation and annealing were carried out *in situ*. After annealing the final PtSi thickness was ≈ 10 nm. Immediately on fabrication the device photoresponse was measured under a reverse bias of 3.5 V as a function of wavelength at $T = 77\,\mathrm{K}$. The Fowler plot of the square root of the photoyield against photon energy yields a barrier height, $\phi_{ph} = 205 \pm 5$ mV[13].

The current–voltage measurements were taken over the temperature range 60–115 K using a Keithley 220 current source and a 3456A HP digital voltmeter. A Cryophysics closed cycle refrigeration system model 22C was used as the low temperature cooling device. Prior to taking I–V measurements, the cryostat was flushed with dry nitrogen gas. It was then pumped to a pressure of 1×10^{-3} torr. In order to avoid condensation on the sample, the cold finger on which the sample was mounted was kept at a higher temperature by activating the heater attached to it and keeping a set point of 300 K during cool down. This allows any residual water vapour, etc., in the cryostat to settle on the radiation shield rather than the cold finger and sample. The radiation shield acts as a cryopump and results in a final pressure less than 10^{-4} torr. A control sensor (silicon diode DT-470) and a control heater were attached, under the base, to the cold finger to monitor and control the temperature to an accuracy of ± 0.1 K using a LakeShore 330 autotuning controller. A second sensor was attached to the top of the base very close to the sample itself to ensure better accuracy in the temperatures measured. The readings from both sensors were within less than 1 K over the entire temperature range.

FORWARD BIAS I–V–T RESULTS AND ANALYSIS

Simple thermionic emission analysis

For each diode studied, 12 I–V–T characteristics were measured in the temperature range 60–115 K. The generally close conformity to linearity of the $\ln\{I/[1 - \exp(-qV/kT)]\}$ vs V plots suggests that the conduction mechanism is essentially thermally activated and that a treatment in which thermionic emission is the dominant current generating mechanism is a useful starting point for the analysis. The I–V relationship in this case is given by[14]:

$$I = I_0 \exp\left(\frac{qV}{nkT}\right)\left[1 - \exp\left(\frac{-qV}{kT}\right)\right], \qquad (1)$$

where I_0, the saturation current, and J_0, the saturation current density, are defined by:

$$J_0 = \left(\frac{I_0}{S}\right) = A^{**}T^2 \exp\left(\frac{-q\phi_j^0}{kT}\right). \qquad (2)$$

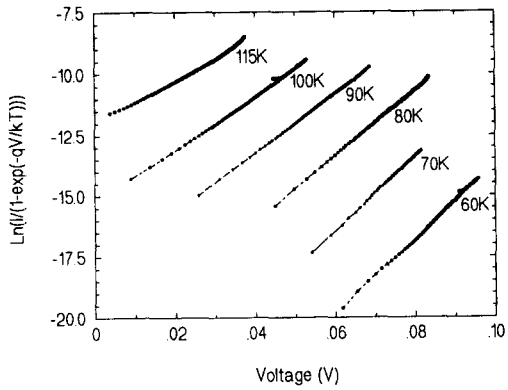

Fig. 1. Plot of $\ln\{I/[1-\exp(-qV/kT)]\}$ against voltage, V, as a function of temperature. Data have been corrected for series resistance according to the method of Boutrit *et al.*[15].

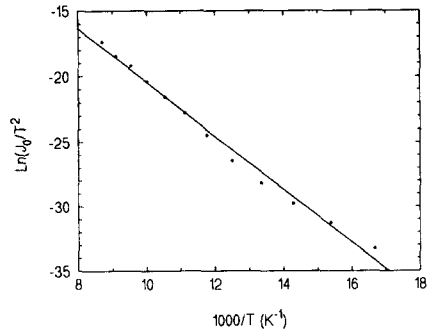

Fig. 3. Richardson plot, $\ln(J_0/T^2)$ against $1000/T$, based on the data of Fig. 1. The gradient yields a value of zero-bias Schottky barrier height, $\phi_j^0 = 177$ mV and the ordinate intercept a value of modified Richardson constant, $A^{**} = 1\ \mathrm{A\,cm^{-2}\,K^{-2}}$.

The quantities S, A^{**}, n and ϕ_j^0 are the diode active area, the modified Richardson constant, the ideality factor and the zero bias Schottky barrier height, respectively. For an applied voltage $V \gg kT/q$ (usually $V \gg 3kT/q$) eqn (1) is usually approximated by:

$$J = J_0 \exp\left(\frac{qV}{nkT}\right). \tag{3}$$

The advantage of retaining the more exact form of eqn (1) is that both I–V data below the $3kT/q$ limit, and reverse bias data may be used. To take the series resistance, R_s, into account, the applied bias, V, in eqn (1) is replaced by $V-R_sI$, thus accommodating the voltage drop across R_s. The effect of the series resistance is factored out of the raw experimental data following the method of Boutrit *et al.*[15]. The corrected data are plotted in Fig. 1 on a semi-logarithmic scale and display linearity of $\ln\{I/[1-\exp(-qV/kT)]\}$ vs V for more than two decades over most of the temperature range. The saturation current, I_0, is obtained from the intercepts of these linear plots with the current axis at $V = 0$. The ideality factor, n, is obtained from the slopes of the same plots and is shown in Fig. 2 as a function of temperature.

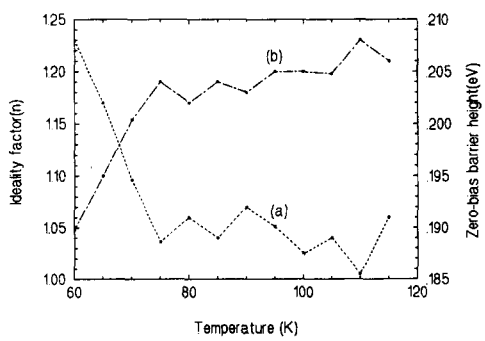

Fig. 2. (a) Ideality factor, n, as a function of temperature. (b) Schottky barrier height, ϕ_j, determined from individual current–voltage characteristics of Fig. 1, as a function of temperature.

If we consider in more detail the characteristic parameters of the conduction process in the Schottky diodes, as described by simple thermionic emission theory, we find there are a number of difficulties. Firstly, although the ideality factor is close to unity over most of the temperature range (60–115 K), it increases significantly as the temperature decreases below 80 K. An ideality factor in excess of unity is usually due to either its bias dependence or to the presence of conduction processes other than pure thermionic emission. Secondly, assuming no prior knowledge of the value of A^{**}, it is necessary to construct a Richardson plot $[\ln(J_0/T^2)$ vs $1/T]$ in order to ascertain values for both A^{**} and ϕ_j^0. The activation energy is given by the gradient of this plot through the relation, derived directly from eqn (2):

$$E_{act} = -k\frac{\mathrm{d}[\ln J_0/T^2]}{\mathrm{d}T^{-1}} = q\left[\phi_j^0 - T\frac{\mathrm{d}\phi_j^0}{\mathrm{d}T}\right]. \tag{4}$$

A Richardson plot is presented in Fig. 3 and shows reasonably good linearity over the whole of the temperature range. Although a straight line is fitted to the data points, there is, significantly, a slight but discernible curvature to the locus of the data points. In effect, in producing a straight line fit we ignore the second, temperature dependent term on the right-hand side of eqn (4). This is in line with normal practice and leads to a value of $\phi_j^0 = 177$ mV from the average gradient or to a value of 192 mV from the gradient at mid-temperature range value of ≈ 90 K. This is a useful starting point for the further development of ideas and analysis. Nonetheless, the curvature that is present is a tell-tale sign of departure from ideal behaviour. Moreover, the values of ϕ_j^0 and $A^{**} \approx 1\ \mathrm{A\,cm^{-2}\,K^{-2}}$, derived from the gradient of the graph and the intercept at $V = 0$, respectively, are rather low. In particular the value for A^{**} is much lower than the values of 32–$43\ \mathrm{A\,cm^{-2}\,K^{-2}}$ previously reported for PtSi/p-Si diodes[9,10]. Thirdly, as an alternative, the barrier height may be determined from the individual $\ln\{I/[1-\exp(-qV/kT)]\}$

vs V plots. If this is done, it is found that ϕ_j^0 decreases with decreasing temperature, as shown in Fig. 2. This feature, along with the curvature in the Richardson plot and the departure of the ideality factor from unity as a function of temperature all amount to different means of representing the underlying diode non-ideality. In summary, several problems arise if simple thermionic emission theory is applied directly to the experimental data.

Non-thermionic emission processes

There is the possibility that these anomalies may be due to other current generation mechanisms such as leakage current, thermionic field emission or recombination. Consider first the possibility of a current component due to leakage. The reverse bias characteristics of the diodes were checked for any leakage behaviour, possibly due to hot spots. The diodes were found to have reverse breakdown voltages beyond -30 V, effectively excluding the possibility of leakage current effects. The importance of a tunnelling current contribution, driven by field emission through a narrow barrier region, may be established by determining the value of the ratio kT/qE_{00} where:

$$E_{00} = 18.5 \times 10^{-12}\left[\frac{N_A}{m_r \epsilon_{sr}}\right]. \tag{5}$$

E_{00} is a parameter which determines the relative importance of thermionic field emission, N_A is the acceptor doping density, m_r is the effective mass expressed in units of the free electron mass and ϵ_{sr} is the static relative permittivity. As a good rule of thumb, field emission is expected if $kT \ll qE_{00}$, thermionic field emission if $kT \approx qE_{00}$ and pure thermionic emission if $kT \gg qE_{00}$. In order to establish the condition for thermionic emission in the most stringent manner, or, in effect, to maximise the possibility of field emission effects, the lowest temperature and greatest doping density are used in the calculation of kT/qE_{00}. For $T = 60$ K, the lowest temperature at which data were taken, and $N_A = 1 \times 10^{15}\,\text{cm}^{-3}$, the upper end of the doping density range in our devices, $kT/qE_{00} \approx 22$. It is therefore clear that field emission effects are insignificant across the temperature range used here. Finally, recombination is also expected to be negligible in these low barrier height diodes[16]. With no significant role for these different current generating mechanisms we are clearly constrained to perform an analysis essentially in terms of the thermionic emission process. However, the thermionic emission model will have to be modified in some way since, as we have already seen, a simple thermionic emission model has various shortcomings.

Modified Richardson plots and the flatband barrier height

In this section, we consider procedures in which the defining equation for thermionic emission is modified in some way to yield a linear, rather than curved Richardson plot. This sort of approach is not physically based, but at least gives some assurance that the results conform to a thermionic emission description, albeit modified. We apply two such procedures to our results here—the so-called T_0-analysis and the construction of a Richardson plot in which the flatband saturation current density is used in place of the zero-bias current density. In the course of the latter approach, we consider the flatband barrier height which may be regarded as the fundamental barrier height.

Schottky barrier contacts which follow a non-perfect thermionic emission model, as is the case here, have frequently been characterized by what is known as the T_0 parameter[17–19]. In this approach, the ideality factor is given by:

$$n = 1 + \frac{T_0}{T}. \tag{6}$$

On plotting nkT/q vs kT/q, it is found to be linear and could be well fitted using $T_0 = 18$ K. In the usual "T_0-analysis" the ideality, n, as given by eqn (6), is introduced also into the denominator of the argument of the exponential function in the expression for the saturation current density [eqn (2)]. When this is done with our data, a plot of $\ln(J_0/T^2)$ vs $1/(T + T_0)$ with $T_0 = 18$ K (as shown in Fig. 4) gives a better straight line fit than the basic activation energy plot presented in Fig. 3. The graph of Fig. 4 yields values of $\phi_j^{T_0} = 258$ mV and $A^{**} = 12.4\,\text{A cm}^{-2}\,\text{K}^{-2}$. Although the T_0-analysis works well, it tends to be unsatisfactory in that its physical significance is ambiguous. Such a temperature dependence of the ideality factor has been variously interpreted in terms of a particular distribution of interface states[17], a non-uniformly doped surface layer[18] and a distribution in the Schottky barrier height[6].

An alternative means of rationalizing the discrepancies of the basic activation energy plot is to use the flatband saturation current density[20], rather than the zero-bias saturation current density. In order to facilitate the development of this approach, and to

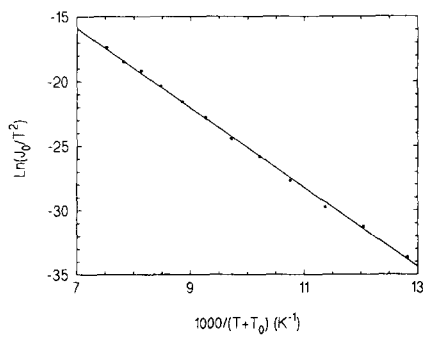

Fig. 4. Modified Richardson plot $\ln(J_0/T^2)$ against $1000/(T + T_0)$ where $T_0 = 18$ K. The gradient yields a value of zero-bias Schottky barrier height, $\phi_j^{T_0} = 258$ mV and the ordinate intercept a modified Richardson constant, $A^{**} = 12.4\,\text{A cm}^{-2}\,\text{K}^{-2}$.

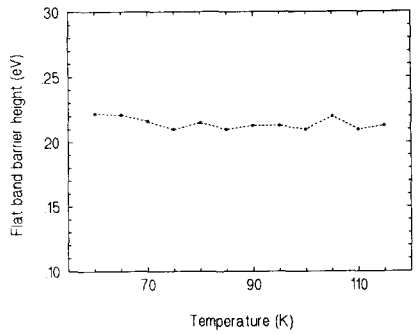

Fig. 5. Flatband barrier height, ϕ_{fb}, as a function of temperature. Gradient of graph or temperature coefficient of flatband barrier height, $\alpha = -0.121\ \text{mV K}^{-1}$.

consider the barrier properties as defined by the experimental results, we need first to consider the flatband barrier height, ϕ_{fb}. This quantity may be considered a fundamental measure of the Schottky barrier height since it normalizes all data to the flatband condition and, in so doing, eliminates the effect of image force lowering. It is defined as[21]:

$$\phi_{fb} = n\phi_j^0 - (n-1)\frac{kT}{q}\ln\frac{N_v}{N_A}, \tag{7}$$

where ϕ_j^0 is the zero-bias barrier height, N_A is the acceptor density and N_V is the effective density of states in the valence band. In addition to the explicit temperature dependence in the equation, note also that N_V is a function of temperature (see ref.[21] for a discussion of this quantity) and that the exact temperature variation of n is implicitly included through use of the experimental results of Fig. 2. As with eqn (5) a value of $N_A = 10^{+15}\,\text{cm}^{-3}$ was used in the calculation. A plot of the flatband barrier ϕ_{fb} as a function of temperature is shown in Fig. 5. Having negated the influence of band bending in the barrier height from the I–V–T data, it is now possible to properly consider the temperature dependence of the barrier. Firstly, it is noted that by comparison with the strongly temperature dependent, zero-bias barrier height, shown in Fig. 2, the flatband barrier height of Fig. 5 is almost temperature independent. Here, its average ($T = 90$ K) value is $\phi_{fb} = 214 \pm 2$ mV. Note that the term "flatband" derives from the zero curvature of the conduction and valence bands in a profile of the potential across the Schottky barrier; the flatband barrier is not defined as being flat with respect to temperature. With regard to the weak temperature dependence that does remain, the temperature dependent barrier height $\phi_{fb}(T)$ may be expressed as:

$$\phi_{fb}(T) = \phi_{fb}^0(T=0) + \alpha T, \tag{8}$$

where $\phi_{fb}^0(T=0)$ is the zero temperature flatband barrier height and α is the temperature coefficient of the barrier height. From Fig. 5 it is found that $\alpha \approx -0.121\ \text{mV K}^{-1}$, in very good agreement with the value given by Werner and Guttler[22], and hence that $\phi_{fb}^0(T=0) = 225$ mV.

In developing the analysis further we follow Unewisse and Storey[23]. Rather than calculating ϕ_{fb} from eqn (7) using values of n and ϕ_j^0 derived on the basis of eqns (1) and (2), we modify these equations by substituting in them the expression for ϕ_j^0 from eqn (7). This leads to a new quantity, the flatband saturation current density:

$$J_{0f} = \frac{I_{0f}}{S} = A^{**}T^2\exp\left(\frac{-q\phi_j^{fb}}{nkT}\right), \tag{9}$$

which is related to the standard or zero-bias saturation current density, J_0, by the equation:

$$J_{0f} = \frac{J_0}{\exp\left[\left(\frac{n-1}{n}\right)\ln\frac{N_A}{N_v}\right]}. \tag{10}$$

From eqn (9), a plot of $\ln(J_{0f}/T^2)$ vs $1000/nT$ should yield a straight line. Figure 6 indeed shows such a linear plot, the gradient yielding a value of $\phi_j^{fb} = 196 \pm 3$ mV.

Inhomogeneous barrier analysis

The procedures developed above, i.e. the T_0-analysis and the use of the flatband saturation current density, serve to linearize the basic Richardson plot. Both are essentially empirical approaches. As a final step in the analysis, we consider a more physical approach, introducing inhomogeneity into the Schottky barrier. A number of groups[5–7,9,24] have recently introduced a spatial distribution in the barrier height to analyse the electrical characteristics for silicide/Si diodes. In particular, Chin *et al.*[9] suggested that for PtSi/p-Si diodes below 80 K the thermionic emission theory should be modified to include a distribution of the barrier height. One of the principal features of such an approach is that, at low temperatures, current flow is strongly influenced by areas of lower barrier height. There are a number of physical considerations which make the introduction of a barrier height distribution plausible and

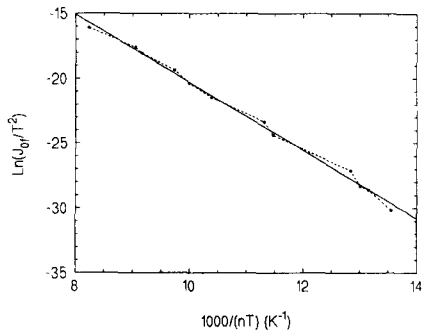

Fig. 6. Modified Richardson plot, $\ln(J_{0f}/T^2)$ against $1000/nT$, where J_{0f} is the flatband saturation current density. The gradient yields a value of zero bias Schottky barrier height, $\phi_j^{fb} = 196$ mV and the ordinate intercept a value of modified Richardson constant, $A^{**} = 12\ \text{A cm}^{-2}\,\text{K}^{-2}$.

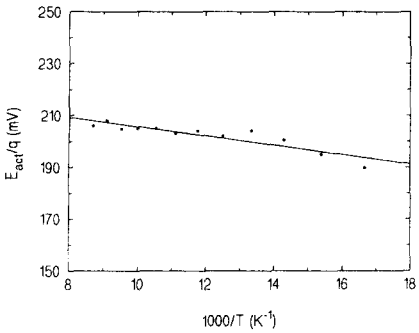

Fig. 7. Activation potential, E_{act}/q, against $1000/T$, based on eqn (14), in accordance with the inhomogeneous barrier model of Ref.[6]. The ordinate intercept gives $T = 0$ barrier height $\bar{\phi}_b^0 = 223$ mV and the gradient leads to value of standard deviation of Gaussian barrier height distribution, $\sigma_\phi = 12.5$ mV.

reasonable. For example, the electrode stoichiometry and atomic structure of the silicide–Si interface are essentially different from those in metal–Si interfaces[25,26]. Silicides are known to grow polycrystalline[25], which may result in interfacial roughening and consequently in local variation of the internal electric field and of the barrier height. In performing an analysis based on barrier inhomogeneity we shall adopt the model of Werner and co-workers[6,7], introducing a Gaussian distribution in the barrier height:

$$P(\phi_b) = \frac{1}{\sigma_\phi (2\pi)^{1/2}} \exp\left(\frac{-(\bar{\phi}_b - \phi_b)^2}{2\sigma_\phi^2}\right), \quad (11)$$

where $\bar{\phi}_b$ denotes the mean barrier and σ_ϕ the standard deviation. The barrier height for zero-bias conditions in eqn (2), ϕ_j^0 is related to the zero-bias mean barrier height $\bar{\phi}_b^0$ and standard deviation σ_ϕ via:

$$\phi_j^0(T) = \bar{\phi}_b^0(T) - \frac{q\sigma_\phi^2}{2kT}, \quad (12)$$

where

$$\bar{\phi}_b^0(T) = \bar{\phi}_b^0(T = 0) + \alpha_\phi T. \quad (13)$$

In this model, we can understand the curved behaviour of the Richardson plot in Fig. 3 as being due to the influence of inhomogeneities. Information on the spatial fluctuations in the barrier height may be extracted by using eqns (12) and (13) in eqn (4) to yield the following equation:

$$\frac{E_{act}(T)}{q} = \left(\bar{\phi}_b^0(T = 0) - \frac{q\sigma_{\phi 0}^2}{kT}\right), \quad (14)$$

and then plotting the activation potential, E_{act}/q, as a function of inverse temperature. When this is done—see Fig. 7—we obtain $\bar{\phi}_b^0(T = 0) = 223$ mV and $\sigma_\phi = 12.5$ mV. The standard deviation is thus $\approx 6\%$ of the total mean barrier height.

DISCUSSION

The various analyses presented above lead to a wide range of barrier heights. It is important to reconcile the differences between these results, in a semi-quantitative fashion at least, and in so doing to understand the input to each analysis and its regime of validity. To assist with the discussion we have summarized the Schottky barrier heights in Table 1 along with the pertinent temperature and bias conditions. In general, a change from one measure of the Schottky barrier height to another involves a change in either the bias and/or temperature conditions. By way of general outline, prior to addressing specific barrier height measurements, we note the consequences of such changes. First, if the temperature is increased, the barrier height reduces in accordance with eqn (8) (α is negative). By contrast, the analysis involving barrier inhomogeneities implicitly assumes that the width of the Gaussian barrier is independent of temperature—from eqn (12) a plot of $(\bar{\phi}_b^0 - \phi_j^0)$

Table 1. Summary of the variously derived Schottky barrier heights, ϕ

Symbol (and origin)	Value (mV)	Conditions
ϕ_{ph} (Photoresponse barrier)	205 ± 5	$T = 80$ K
ϕ_j^0 (Richardson plot based on raw I–V–T data)	192 (130–194)	Ave T (≈ 90 K) value Zero bias
$\phi_j^{T_0}$ (Modified Richardson plot based on T_0-analysis)	258 ± 5	$T_0 = 18$ K Zero bias
$\phi_{fb} = \phi_{fb}^0(T = 0) + \alpha T$ (Flatband analysis)	214 ± 3 $\alpha = -0.121$ mV K^{-1}	Ave T (≈ 90 K) value Flatband condition (Forward bias $V = \phi_{fb}$)
ϕ_j^{fb} (Modified Richardson plot based on flatband saturation current)	196 ± 4	Ave T (≈ 90 K) value Flatband saturation current
$\bar{\phi}_b^0(T = 0)$ (Mean barrier height in inhomogeneous barrier model) where $\bar{\phi}_b^0 = \bar{\phi}_b^0(T = 0) + \alpha_\phi T$	223 ± 4	$T = 0$ Zero bias
σ_ϕ where $\sigma_\phi^2 = 2kT/q(\bar{\phi}_b^0 - \phi_j^0)$	12.5	

against $1/T$ will yield a straight line of gradient $q\sigma_\phi^2/2k$. This does not mean to say that the barrier distribution does not influence the perceived Schottky barrier height—at low temperatures, for example, current transport across the low barrier regions will be relatively more important in determining the barrier height.

Second, a change in bias will affect the barrier height in two ways. In progressing from the flatband condition to zero bias and then reverse bias, image force lowering becomes increasingly important, in accordance with the equation[27]:

$$\Delta\phi = \left[\frac{q^3 N_A}{8\pi^2(\epsilon_s')^2\epsilon_s}\right]^{1/4}\left[\phi - V - \xi - \frac{kT}{q}\right]^{1/4}. \quad (15)$$

Here, the previously undefined quantities ξ and ϵ_s are the separation between the Fermi level and the valence band edge and the (static) dielectric constant of the semiconductor, respectively (ϵ_s' is the high frequency dielectric function; here we take $\epsilon_s = 11.7\epsilon_0$ and $\epsilon_s' \approx 12\epsilon_0$). The barrier height, ϕ, in the equation above may be identified here with the flatband barrier height. In addition, in the inhomogeneous barrier model of Ref.[6], the standard deviation of the barrier distribution is shown to be voltage dependent in such a way that it decreases (to zero in principle) on approaching the flatband condition. Physically, this phenomenon may be linked to the shift of the barrier maximum into the semiconductor substrate, away from the metal/semiconductor interface itself. It has further been argued that the local electromagnetic interactions involved in the collapse of the distribution spread lead to the lower barrier regions being pinched off[7]. This narrowing of the distribution as the applied voltage approaches the flatband voltage, possibly combined with an upward movement of the mean barrier height as the lower regions are "pinched off", means that any measurement of the barrier height based on I–V–T measurements should tend to higher values with increasing voltage. Sensitivity of the barrier to the voltage dependent value of σ_ϕ is greater at lower temperatures where the lower barrier height regions make a relatively more significant contribution to the current transport process.

First, let us consider the barrier heights yielded by the photoresponse measurements, ϕ_{ph}, and by the basic I–V–T data, ϕ_j^0. The values cited in Table 1 are for almost the same temperature, but for quite different bias conditions. Relative to the flatband case, the zero bias conditions pertinent to the (extrapolated) saturation current densities of Fig. 3 would imply, according to eqn (15), image force lowering of 9 mV, while the relatively large reverse bias of -3.5 V (and thus significant band bending implied in the photoresponse measurements) would lead to a lowering of 20 mV. Thus, on the grounds of image force considerations, ϕ_{ph} ought to be less than ϕ_j^0 by ≈ 11 mV. In fact, the disparity between the two measurements is slightly larger (13 mV) and the other way round—this is a feature which has been noted previously[9]. To explain the discrepancy we appeal to hot carrier scattering in the PtSi electrode[28]. This phenomenon means that fewer charge carriers in the metal electrode, holes in our case, successfully reach and negotiate the barrier than would be the case ideally. Consequently, in a Fowler plot of the square root of the photoyield against photon energy, the photoyield data are suppressed to lower values, pushing the energy axis intercept, which determines the barrier height, to a higher value. An analogous argument does not apply to the transport of majority carriers across the barrier from semiconductor to metal electrode relevant to the I–V–T data. This intrinsic asymmetry between the two types of measurement means that the photoemission data yield a greater barrier height than the I–V–T data. There does, however, remain something of a gap between $(\phi_{fb} - \Delta\phi) = 205$ mV and the current barrier height, $\phi_j^0 = 192$ mV at $T = 90$ K. Here, we appeal to the finite, voltage dependent barrier distribution (standard deviation $\sigma_\phi = 12.5$ mV for zero bias conditions) to reconcile the difference. The displacement between the two values amounts to just about one standard deviation of the (assumed) Gaussian barrier height distribution.

We now pass comment on the various Richardson plots. The two modified plots (Figs 4 and 6) provide a better straight line fit of the $\ln(J_0/T^2)$ data as a function of inverse temperature than the unmodified Richardson plot of Fig. 3. The barrier activation energy, taken directly from the gradient for such plots [eqn (4)] thus becomes uniform across the temperature range. In the first case, the T_0-analysis (see Fig. 4), the temperature axis of the raw Richardson plot is, in effect, compressed non-linearly with larger relative reductions for high values of inverse temperature. This action linearizes the plot and yields a somewhat steeper gradient or higher value for the Schottky barrier, $\phi_j^{T_0} = 258$ mV, than the unmodified data of Fig. 3. The value of the Schottky barrier height, $\phi_j^{T_0}$ is rather high for the type of diode examined here but, because of the empirical type of procedure used, it is not of particular physical significance.

In the second modified Richardson plot (Fig. 6) the flatband saturation current is used. In essence the $\ln(J_0/T^2)$ axis of the basic Richardson plot is modified in a non-linear fashion *in addition* to the same non-linear scaling of the inverse temperature as is used in the T_0-analysis. [So far as the inverse temperature axis is concerned, the only difference is that the T_0-analysis uses a modelled value for the ideality factor n—given by eqn (6)—whereas the flatband saturation analysis uses the experimental values for n; the two are, however, in good agreement, so that the scaling of the inverse temperature in the two cases under discussion is essentially identical.] In general, this leads to an improved linearization of the data or superior uniformity of the Schottky barrier height across the temperature range;

indeed the linearity of such plots can be truly impressive[23]. However, J_0 converts to J_{0f} according to eqn (10) in such a way that there are smaller relative changes to J_0 for higher temperatures. Hence, the gradient of the modified Richardson plot, and thus the Schottky barrier height ($\phi_j^{fb} = 196$ mV), is less than that yielded by the T_0-analysis ($\phi_j^{T_0} = 258$ mV), falling between that and the barrier height, $\phi_j^0 = 192$ mV ($T \approx 90$ K) of the basic Richardson plot. The flatband barrier height itself, $\phi_{fb} = 214$ mV, calculated directly from eqn (7) is such that $\phi_j^0 < \phi_j^{fb} < \phi_{fb}$. The ordering of these barrier heights is the same as that found by Unewisse and Storey[23] who first introduced the flatband saturation current analysis in the context of their investigation of erbium silicide/silicon diodes—for the record those authors found $\phi_j^0 = 276$ mV ($T > 70$ K), $\phi_j^{fb} = 281$ mV and $\phi_{fb} = 283$ mV.

The two most fundamental current barrier heights in Table 1 are the flatband barrier height, $\phi_{fb} = 214$ mV, and the mean barrier height at $\bar{\phi}_b^0(T = 0) = 223$ mV, derived on the basis of the inhomogeneous barrier model. Are these two values for the Schottky barrier height consistent? In the first place ϕ_{fb} is an average barrier height over the range of temperature measurements and therefore corresponds to a temperature of ≈ 90 K. Assuming a linear temperature coefficient, $\alpha = -0.121$ mV K^{-1} [eqn (8) and Fig. 5], this barrier would increase by 11 mV to 225 mV at $T = 0$ K, thus aligning well with $\bar{\phi}_b^0(T = 0)$, valid for the condition $T = 0$ K. However, there is also an effective change in applied bias conditions between the two barrier heights. Let us now notionally keep $T = 0$ K and align the bias condition pertinent to the mean barrier height to that for the flatband barrier height. The value of $\bar{\phi}_b^0(T = 0)$ is implicitly a zero-bias barrier height through eqns (4), (12) and (13). In a simple view, one would argue that in moving from the zero bias to the flatband condition, image force lowering is undone. According to eqn (15), if a flatband bias of 158 mV is applied, this should happen to the tune of 9 mV, thus largely undoing the alignment due to the effect of the implied temperature change. The flatband and mean barrier height (at flatband bias) at $T = 0$ K would thus be 225 and 232 mV, respectively. However, in the model[6] underpinning the inhomogeneous barrier analysis, the voltage dependencies of the mean barrier height and of the barrier distribution width are given, respectively, by coefficients ρ_2 and ρ_3 which are related to the ideality factor by the equation

$$\frac{1}{n} - 1 = -\rho_1 = -\rho_2 + \frac{\rho_3}{2kT/q}. \qquad (16)$$

Indeed one of the central features of this model is that it identifies the ideality factor n as a representation of the voltage deformation of the barrier distribution at an inhomogeneous interface. There are two component parts to this deformation, one the change in mean barrier height, characterized by the parameter ρ_2, and the other, the change in the width of the distribution characterised by ρ_3. (For a detailed development of this equation see Ref.[6].) It turns out that the value of ρ_2 is negative, not only in the data of Werner and Guttler[6] (for PtSi/n-Si samples) but in the data of other investigations which they analyse and in the data presented here. This implies that the mean barrier height should decrease with increasing forward bias, which is in the opposite sense to image force lowering! (It is thus not clear physically to us why the value of ρ_2 should be negative in this model.) The overall increase of barrier height with increasing bias, within this model, is entirely due to the narrowing of the barrier potential distribution, as described by a negative value of ρ_3. Again, in all cases alluded to above, the value of ρ_3 is indeed negative and sufficiently so that the overall voltage dependence of the barrier height, given by ρ_1, is positive. Here, with a value of $\rho_1 \approx 0.05$ the increase in barrier height with increasing bias (from zero to flatband bias) is ≈ 8 mV. This is slightly less than the estimate based on the image force effect giving a value of 231 mV for the mean barrier height under flatband bias and at $T = 0$ K. Ideally we would like this value to align with $\phi_{fb}(T = 0) = 225$ mV but a small discrepancy remains.

To summarize at this stage, we note that the barrier heights derived from the modified Richardson plots are different from each other and from the flatband barrier height. While we do not attempt to attach physical interpretations to these barrier heights we nonetheless note that linearity in both the modified Richardson plots, particularly that utilizing the flatband saturation current, serves as an excellent check on the validity of viewing the I–V–T data in the framework of a modified thermionic emission model. For the same temperature and bias conditions, the flatband barrier height, ϕ_{fb}, and the mean barrier height of the inhomogeneous barrier model agree to within less than 10 mV. In principle, the flatband barrier height at $T = 0$ K and the mean barrier height at flatband bias and $T = 0$ K should be regarded as the most fundamental measures of the Schottky barrier height. From the inhomogeneous barrier model we note that the standard deviation in the assumed Gaussian barrier distribution, $\sigma_\phi = 12.5$ mV, is in good agreement with the value of 11 mV, also for PtSi/p-Si diodes, found by Chin *et al.*[9] who used an iterative, numerical technique in modelling the barrier inhomogeneity, rather than the more analytical model of Ref.[6] adopted here. (We note, though, that the reported mean barrier height is ≈ 12 mV greater in the work of those authors than in the present investigation.) Finally, we remark that measurable evidence of barrier inhomogeneity implies that the inhomogeneities in our diodes are on a scale greater than the Si Debye length. Ohdomari and Aochi[29] have argued that if the scale of the inhomogeneities is less than the Si Debye length then they have essentially no influence on the barrier height—the

current transport properties of the barrier would be essentially determined only by the low barrier regions.

Finally, we consider briefly the implications of the value of the temperature coefficient of the flatband barrier, $\alpha = -0.121$ mV, evaluated on the basis of Fig. 5. Tersoff[30] proposed that the p-type Schottky barrier height is given by:

$$\phi_{bp} = \frac{1}{2}\left(E_g^i - \frac{\Delta}{3}\right) + \delta_m, \qquad (17)$$

where E_g^i is the semiconductor indirect band gap, Δ is the spin-orbit splitting ($\Delta = 40$ mV for Si), and δ_m is an adjustable parameter. This relationship is based on the Fermi level being pinned to the centre of the semiconductor indirect band gap, and it predicts that both n-type and p-type barrier heights decrease with increasing temperature with the same coefficient. This coefficient is equal to $1/2(dE_g^i/dT)$, i.e. half the temperature coefficient of the indirect band gap itself. Comparing the value of ≈ -0.2 mV K^{-1} for dE_g^i/dT for Si with the barrier temperature coefficient $\alpha = -0.121$ mV K^{-1} obtained in this work, we conclude that the Fermi level is pinned to the centre of the indirect band gap. Werner and Guttler[22] found similar behaviour for Pd_2Si and $CoSi_2$ as well as for PtSi, as Aboelfotoh *et al.*[31] did for Ti and its silicide $TiSi_2$. This is in contrast with Chin and Storey[32]; they proposed that the barrier height was pinned to the valence band edge. By contrast, other silicides appear to exhibit pinning relative to the valence band edge—for example, WSi_2 (Aboelfotoh[33]) and $CoSi_2$ (Duboz *et al.*[34])—or the conduction band edge—here we may cite the case of $ErSi_2$ on Si(111). Aboelfotoh[33] has postulated that the change in Fermi level pinning from below to near the gap centre, and then to above the gap centre and the parallel and consequent change in $d\phi_{bp}/dT$ from ≈ 0 to $1/2(dE_g^i/dT)$, and finally to $\approx dE_g^i/dT$, is dependent on the metal electronegativity. Here, we reiterate that our results are consistent with pinning of the Fermi level relative to the middle of the Si indirect band gap.

CONCLUSIONS

The forward current conduction characteristics of moderately doped PtSi/p-Si Schottky barrier diodes have been studied over the temperature range 60–115 K. The basic Richardson plot (Fig. 3) actually displays a slight but significant curvature and yields low values for ϕ_J^0 (192 mV at $T \approx 90$ K) and A^{**} (1 A cm^{-2} K^{-2}). The disparity between this basic barrier height and that yielded from photoemission data ($\phi_{ph} = 205$ mV) may be reconciled in terms of an explanation based on hot carrier scattering in the PtSi electrode. The flatband barrier height, ϕ_{fb}, a fundamental measure of the Schottky barrier which eliminates the effects of image force lowering, is calculated from the I–V–T data to be 214 mV with a negative temperature coefficient, $\alpha = -0.121$ mV K^{-1}.

The curvature of the basic Richardson plot may be substantially remedied in an empirical manner by introducing the so-called T_0-parameter, with an optimum value here of $T_0 = 18$ K. Alternatively, following the procedure of Unewisse *et al.*[23] the flatband barrier height expression may be used to define a flatband saturation current density, J_{0f}, which in turn is used to construct a modified Richardson plot in which, relative to the unmodified plot of Fig. 3, both the ordinate and the inverse temperature axes are scaled non-linearly. Both the modified Richardson plots described above indicate that the data can be explained in the framework of a modified thermionic emission behaviour. A more physical basis to the departure from ideal thermionic emission is given in terms of an inhomogeneous (Gaussian distributed) barrier model[6,7] in which the barrier height is found to have a zero bias, zero temperature mean value, $\bar{\phi}_b^0(T=0) = 223$ mV with a standard deviation $\sigma_\phi = 12.5$ mV. Taking into consideration the relevant bias and temperature conditions, this barrier height and the flatband barrier height can be reconciled to within about 6 mV. Finally, it is noted that the value of the flatband temperature coefficient indicates that the Fermi level at the interface is pinned relative to the middle of the Si indirect band-gap.

Acknowledgements—This project was supported jointly by funding from the United Kingdom Science and Engineering Research Council (grant refs GR/G24255 and GR/K76078) and the Technology Board for Northern Ireland (grant ref. ST57 QUB). P.G.McC. would also like to acknowledge the support of a Co-operative Award in Science and Technology funded by the Department of Education for Northern Ireland and the Northern Telecom NITEC Centre, Northern Ireland, U.K.

REFERENCES

1. P. W. Pelligrini, C. E. Ludington and M. M. Weeks, *J. appl. Phys.* **67,** 1417 (1990).
2. A. Kikuchi, T. Ohshima and Y. Shiraki, *J. appl. Phys.* **64,** 4614 (1988).
3. A. Kikuchi, *J. appl. Phys.* **74,** 3270 (1993).
4. A. Tanabe, K. Konuma, N. Teranishi, S. Tohyama and K. Masubuchi, *J. appl. Phys.* **69,** 850 (1991).
5. H. H. Guttler and J. H. Werner, *Appl. Phys. Lett.* **56,** 1113 (1990).
6. J. H. Werner and H. H. Guttler, *J. appl. Phys.* **69,** 1522 (1991).
7. J. H. Werner, H. H. Guttler and U. Rau, *Mat. Res. Soc. Symp. Proc.* **260,** 311 (1992).
8. M. O. Aboelfotoh, *J. appl. Phys.* **69,** 3351 (1991).
9. V. W. L. Chin, M. A. Green and J. W. V. Storey, *Solid-St. Electron.* **33,** 299 (1990).
10. V. W. L. Chin, M. A. Green and J. W. V. Storey, *Solid-St. Electron.* **36,** 1107 (1993).
11. A. Sellai, P. G. McCafferty, P. Dawson, S. H. Raza and H. S. Gamble, *Infrared Detectors: State of the Art I* (Edited by W. H. Makky). *Proc. SPIE* **1735,** 240 (1992).
12. A. Sellai, P. G. McCafferty, P. Dawson, S. H. Raza and H. S. Gamble, *Int. J. Optoel.* **19,** 65 (1994).
13. A. Sayed, Fabrication and photoemission measurements were performed at Loral Fairchild Imaging Systems (Milpitas, CA). Internal report.

14. E. H. Rhoderick and R. H. Williams, *Metal–Semiconductor Contacts*, 2nd Edn, p. 39. Oxford University Press (1988).
15. C. Boutrit, J. C. Georges and S. Ravelet, *IEE Proc.* **127,** 250 (1990).
16. E. H. Rhoderick and R. H. Williams, *Metal–Semiconductor Contacts*, 2nd Edn, p. 118. Oxford University Press (1988).
17. J. D. Levine, *J. appl. Phys.* **42,** 3991 (1971).
18. C. R. Crowell, *Solid-St. Electron.* **20,** 171 (1977).
19. C. R. Crowell and V. L. Rideout, *Solid-St. Electron.* **12,** 28 (1973).
20. L. F. Wagner, R. W. Young and A. Sugerman, *IEEE Electron Device Lett.* **4,** 320 (1983).
21. S. M. Sze, *Physics of Semiconductor Devices*, 2nd Edn, p. 81. Wiley, New York (1981).
22. J. H. Werner and H. H. Guttler, *J. appl. Phys.* **73,** 1315 (1993).
23. M. H. Unewisse and J. W. V. Storey, *J. appl. Phys.* **73,** 3873 (1993).
24. P. Niedermann, L. Quattropani, K. Solt, A. D. Kent and O. Fischer, *J. Vac. Sci. Technol. B* **10,** 580 (1992).
25. H. B. Ghozlene, P. Beaufrere and A. Authier, *J. appl. Phys.* **49,** 3998 (1978).
26. P. E. Schmid, P. S. Ho, H. Foll and T. Y. Tan, *Phys. Rev. B* **28,** 4593 (1983).
27. E. H. Rhoderick and R. H. Williams, *Metal–Semiconductor Contacts*, 2nd Edn, p. 36. Oxford University Press (1988).
28. J. M. Mooney, Ph.D. Thesis, University of Arizona (1986).
29. I. Ohdomari and H. Aochi, *Phys. Rev. B* **35,** 682 (1987).
30. J. Tersoff, *Phys. Rev. Lett.* **52,** 465 (1984); *Phys. Rev.* **32,** 6968 (1995).
31. M. O. Aboelfotoh and K. M. Tu, *Phys. Rev. B* **34,** 2311 (1986); M. O. Aboelfotoh, *J. appl. Phys.* **64,** 4046 (1988).
32. V. W. L. Chin and J. W. V. Storey, *J. appl. Phys.* **68,** 4127 (1990).
33. M. O. Aboelfotoh, *Solid-St. Electron.* **34,** 51 (1991).
34. J. Y. Duboz, P. A. Badoz, F. Arnaud d'Avitaya and E. Rosencher, *J. Elec. Mat.* **19,** 101 (1990).